Vortex Particle-Mesh simulations of Vertical Axis Wind Turbine flows: from the blade aerodynamics to the very far wake
Reply to reviewers

P Chatelain[a], M Duponcheel[a], D-G Caprace[a], Yves Marichal[b], G Winckelmans[a]

[a] *Institute of Mechanics, Materials and Civil Engineering, Université catholique de Louvain, 1348 Louvain-la-Neuve, Belgium*
[b] *Wake Prediction Technologies (WaPT), Rue Louis de Geer 6, 1348 Louvain-la-Neuve, Belgium*

1. Introduction

First and foremost, the authors wish to thank the reviewers for their time, their careful review, and their appreciation of the work. We are most grateful for the insightful comments, which we have addressed thoroughly below and in the revised paper. We hope this will satisfy the reviewers.

2. Reviewer 1

Below we reply to every point brought by this reviewer. The corresponding changes are highlighted in blue in the revised manuscript; changes that address a comment common to both reviewers are shown in orange.

Comment 1. In Figure 1, please provide some explanation for the discrepancy in the two experimental measurements of tangential force coefficient near theta=90 degrees for tsr=2 and near 135 degrees for tsr=4.5. In the prior case, the error bars in the measurements do not overlap, which casts doubt on these data and confused at least this reader.

As stated by the author of the experiment in their conclusions [1]: "the load determination method is unreliable at this position, since the blade is in deep stall. The momentum was not conserved, what creates large variations on the loads for the different contours, resulting in an error on the mean load value. This azimuth position can not be used for comparisons in tangential direction." However, we agree with the reviewer that the non overlapping, large error bars are confusing, and a comment on the validity of experimental data at these specific angular position could be done. The following modification will be brought to the text: "The experimental points hint at a stall happening later on the upstream stretch, around $90°$, and more abruptly than for the simulation; we report here that the authors of the experiment advised to use circumspection for the F_n data at $135°$ and clearly question the validity of their results for F_t through the whole rotation. We nevertheless confront our simulations to all their results in Fig. 1."

Comment 2. Please provide the Reynolds number for the VAWT flow that is being studied. There should also be some discussion on the state of the initial shear layers and tip vortices. Are these expected to be initially laminar or turbulent, based on the flow Reynolds number? Is the SFS model active in the early wake shear layers/vortices? Are these initial flow structures in a transitional regime, and if so, how much confidence do you have in the ability of the LES model to correctly predict transition from an initially laminar to turbulent state? Might this affect some of the behavior of the wake instability and subsequent breakdown?

We agree with the reviewer to say that the original text contained only little information about the transition to turbulence.

- The Reynolds number based on the chord of the blades and on the tangential velocity $U = \omega R$ amounts to $Re = 4.0\,10^5$. In that regime, we would expect the boundary layers to be transitional or turbulent, and thus the shear layers to rapidly grow turbulent downstream of the blades. The resolution of the current simulations and the current implementation of the lifting line in the Vortex Particle Mesh method do not allow to capture fine scale perturbations within the shed vortical structures; only the "larger scales" of the shed vortex sheets are captured, in the form of spanwise and streamwise vorticity components due to the spatial and temporal variations of lift. These vortex sheets are thus generated in a laminar way; they are however sensitive to core size instabilities: starting or end effects due to temporal variations, internal waves (Kelvin modes),...

We have added a mention of the blade Reynolds number and a brief contextual remark about the limitations of the lifting line approach in the section concerning the lifting lines: "We note that all these methods are not able to capture the sub grid scale structure of the actually shed structures."

- Our Sub-Grid Scale (SGS) model is actually acting on the small resolved scales of the flow following the *complete-small* Reduced Variational Model (RVM) implementation. This means that turbulence modeling is acting on the shed structures directly behind the blade, albeit in a very controlled fashion, and thus does not dissipate them too quickly.

- Although the initial flow structure are shed in a laminar like manner, we do believe that our simulations correctly capture the transition to a fully developed turbulent wake. The above-mentioned lacking internal perturbations have no effect on the large-scale trajectories of the vortices, which are precisely governing the vortex-vortex interactions and reconnections. As they generally occur between vortices of different intensities, these events are very intense and produce a great amount of stretching, actually overwhelming the generation of small scales and turbulence.

  As the interactions are more frequent at the corner of the wake, the transition to turbulence is propagating from those regions to the rest of the wake, what we meant to say when writing: “As a direct consequence, the turbulent regions of the wake grow from the corners and the wake only reaches a fully turbulent state once these regions have merged.” We propose the following modification to clarify the relation between vortex interactions and transition: “In this kind of event, the stronger vortex distorts the weaker one, leading to intense stretching, enstrophy production, and the propagation of disturbances along the vortex cores therefore bringing an overwhelming contribution to the transition to turbulence.” See also answer to comment 6 of Reviewer 2.

In conclusion, we do not think that the absence of an accurate prediction of the shear layer transition will affect the behavior of wake decay. The wake instabilities, and more generally the wake dynamics, are governed by the circulation of the vortices which we do capture. This dictates the growth rate of instabilities (at least, to the leading order). Nevertheless, we are currently considering the improvement of our lifting line model to also capture the shear layers originating from the blades. A more thorough analysis of the influence of the shear layers on the transition mechanisms will then be possible.

Comment 3. Related to the previous point, does Figure 6 show the resolved TKE, or total TKE (resolved+modeled)?

Figure 6 shows resolved TKE only; this is now mentioned in the caption.

Comment 4. In paragraph 10, Page 12, there is a discussion on the possible presence of mean streamwise vortices through investigation of the velocity and TKE fields. Why not look at the streamwise vorticity field directly?

Mean streamwise vorticity field is difficult to interpret because of the nearly perfectly periodic behavior of that quantity in the wake. Even with converged statistics, we observe seemingly noisy patches of axial vorticity of opposite signs, with no clear conclusion to be drawn regarding the dominating streamwise component (see Fig. 1 for example). We now have included such plots and added a short discussion in the text at the end of the discussion of averaged flow quantities: The mean streamwise vorticity at three transverse slices is shown in Fig. X. Even though the statistics are converged, the near-perfect periodicity of the flow leads to a pattern of positive and negative patches, signatures of the advection of tip vortices shed on the upstream and downstream parts of the rotation, respectively. The dominant streamwise vorticity is thus difficult to identify in the near-wake but large scale structures can be identified further downstream, also thanks to the induced deformation of the wake.

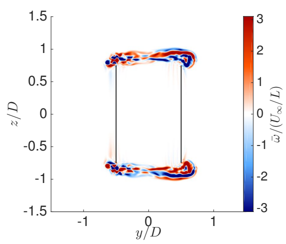

(a) $x/D = 1$

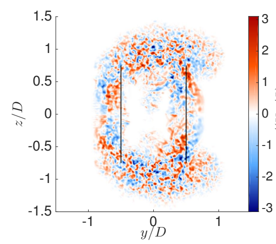

(b) $x/D = 5$

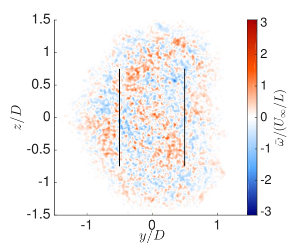

(c) $x/D = 10$

Figure 1: H-type VAWT with $AR = 1.5$: mean streamwise vorticity $\bar{\omega}/(U_\infty/L)$.

3. Reviewer 2

Below we reply to every point brought by this reviewer. The corresponding changes are highlighted in green in the revised manuscript; changes that addressed a comment common to both reviewers are shown in orange.

Comment 1. The title of the paper as a sub-title: "from the blade aerodynamics to the very far wake". The actuator/lifting line method does not present detail at chord level; therefore, although the model is suitable for blade scale aerodynamics, the current formulation of the title is not accurate. The analysis is limited to eight diameters downstream, for which the reference to "very far wake" is not accurate. I suggest revising the title.

We partially agree with the reviewer on that comment. On the first remark, we totally agree: the lifting line model does not represent detailed aerodynamics and therefore, the original title of the manuscript can be misleading. On the second remark, however, we disagree. Our results and analyses entail features up to as far as 15 diameters downstream. Regarding most of today's literature concerning VAWT, this can be considered as "very far wake".

We consider that the formulation "blade scale aerodynamics", suggested by the reviewer, is more suitable to our method; we propose to go even further with the completely unambiguous: "airfoil performance",

Therefore, we would change from the original title to: "Vortex Particle-Mesh simulations of Vertical Axis Wind Turbine flows: from the airfoil performance to the very far wake"

Comment 2. Abstract: the authors mention very long distances?. I suggest a more precise characterization, as for example, up to 8 diameters downstream?.

In line with our answer to the previous comment, we consider consider the following modification: “The complex wake development is captured in details and up to 15 diameters downstream: [...]”

Comment 3. P5, fig 1 and its discussion, it is stated that for TSR=4.5, the results compare well with experiments, although Fn is clearly underpredicted.

This is true and we are grateful to the reviewer for this remark. The discrepancy is in fact quite visible at high TSR: the machine is then more loaded and the visited angles of attack are in a smaller range than in the low TSR case. We attribute it to the curvature of the relative flow, which is not sensed by the standard lifting line method, but which in reality tends to increase the loading of the blade [2]. In our comparison with Castelein's experiment [1], flow curvature was not taken into account nor modeled. Such a correction is not very complicated to add and it was in fact introduced in our lifting line model in later simulations of the Castelein VAWT. We had not reported on this correction in the original manuscript due to format constraints. The correction, for a VAWT, consists in virtually increasing the angle of attack of the blade by an amount which we compute using the radius of the turbine, the chord of the blade and thin profile theory considerations.

In the new version of the manuscript, we add results with curvature correction in the Validation section, which do confirm our suspicion above and dramatically improves our results. A paragraph has been added in the section devoted to the lifting line: The standard lifting line and the actuator line techniques are not able to capture flow curvature effects. Indeed, if the flow relative to the blade is curved, as it is the case here for a blade in rotation through essentially straight streamlines, the airfoil behaves as an airfoil with an additional camber [3, 4]. We consider a blade with a chord c tangentially positioned at a radius R for its quarter-chord position, this additional camber can be modeled in a straightforward manner by pitching the blade inwards by an angle $\alpha_0 =$

$\arctan\left((1-\cos(\beta/2))/\sin(\beta/2)\right)$ where $\beta = \arctan(c/2\,R) + \arctan(c/2\,R)$. In the validation section below (Sec 3.1), we verify the positive effect of such a correction.

The following discussion has been added in the validation section: We report on VPM simulations with and without a curvature correction, which here amounts to a inward pitch $\alpha_0 = 1.72°$. This correction appears to bring a notable improvement of the results particularly for the moderate TSR: the explored angles of attack are indeed smaller than at low TSR.

Finally, we make clear that the production simulations of sections 3.2, 3.3 etc. do not include this correction: Simulations of these sections were run without the curvature correction investigated above (or equivalently, the simulated corresponds to a machine with a blade pitched outwards by $\alpha_0 = 1.65°$).

Comment 4. P7, the maximum angle of attack are not at $\theta = 90$ and 270 degrees

---

The maximum angle of attack are in the vicinity of $\theta = 90$ and 270 degrees. "The tip vortices are the strongest in the vicinity of the upstream- and downstream-most positions of the blades (around $\theta = 90°$ and $270°$) where the blades operate at their maximum angle of attack."

Comment 5. P9, "At the design TSR, the blade exploits the delayed stall at its most:" – please explain what this means.

What we meant is that in this regime (at the design TSR), there is an optimum between the delay on the circulation development and the occurence of airfoil (deep) stall. Here is the qualitative explanation of the trade off. Due to dynamic stall, the maximum angle of attack, circulation and thus normal force occur after the passage of the maximum of geometric angle of attack ($\theta = 90°$ and $270°$), and this benefit is increasing as long as the TSR decreases. However, decreasing the TSR also means increasing the max value of the AoA. At some point, leading edge vortex shedding will occur (which is here beneficial), but the lower the TSR, the sooner it will appear, and so the shorter the delay before the circulation drops (after the leading edge vortex passage). This phenomenon can be observed in Figure 3b, which shows the normal force (and thus the circulation) drop dramatically just before 90°. We note that the drop location is in agreement with the expected behavior of the Dynamic Stall model and parameters.

We consider the addition of the following clarification: "At the design TSR, the blade exploits the delayed stall at its most: its circulation keeps increasing, well past $\theta = 90°$, and then smoothly decreases. This is explained by two phenomena: (1) the airfoil experiences the highest delay in the circulation development (beneficial in this case as it widens the extent of torque production by the blade); (2) the leading edge vortex does not introduce a sharp drop in circulation yet (which clearly happens at lower TSR, see Fig.3b)."

Comment 6. P9, "this mechanism, most visible in fig 4a, is well known in vortex dynamics and had already been identified on aircraft wakes." I suggest a figure where you highlight this event. It is a too complex process for a reader to follow form this short description.

We propose the addition of the figure here labeled 2, to illustrate the vortex interactions.

Comment 7. P9, "One needs to add additional terms to enforce an outflow conditions for this otherwise clipped vorticity field; the present study does precisely that by enforcing a normal outflow velocity through its Fourier-based

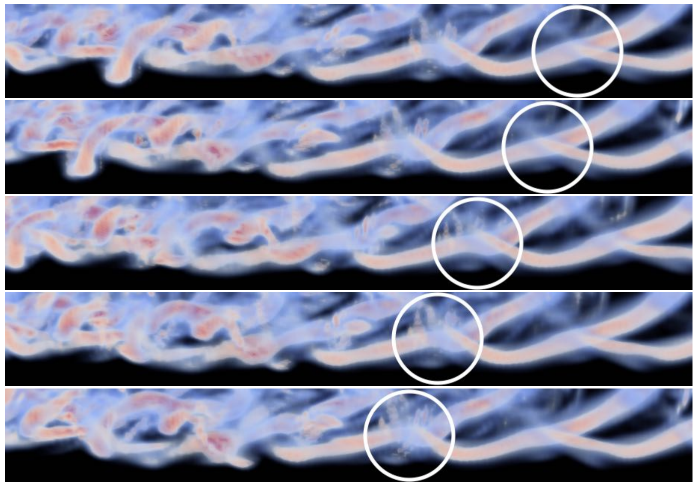

Figure 2: Vortex interactions are visible on the side of the wake, here illustrated in the area behind the bottom left corner of the VAWT, at successive times. The turbine is on the right, and the velocity is directed to the left.

solver.? This explanation is not clear. a. The comparison with the work of Scheurich uses TSR as a term of comparison; wouldn't loading be a more relevant term? The strength of the tip vortex is dependent also on the airfoil used; are these comparable? b. Other authors have used free wake vortex filament models, and have seen the same effect of inboard motion. How does this hold with the suggestion that a term should be added to the FFT solution in a meshed domain?"

This meant to say that, contrarily to other methods like free vortex filaments methods, the outflow conditions does not simply consist in clipping the vorticity. In our case, outflow boundary conditions are applied on the velocity field at the outflow plane. In the present case, these specific conditions are chosen so that the velocity field at the outflow plane is purely normal.

- We agree with the reviewer that the loading is a relevant parameter for comparison. Initially, we were expecting that, the loading being so closely linked with TSR, we wouldn't be too far from Scheurich's loading by using the same TSR.

- The airfoil used is the same as for Scheurich's experiment. More precisely, we are using the very same Dynamic Stall model with the same coefficients. However, in the present simulations, the pitching angle was not adapted in order to take into account an effect of curvature of the relative flow (see answer to comment 3) and it is not clear whether Scheurich et al. are doing it too. This generates an uncertainty with respect to the loading of the blade as a function of the TSR, which points toward the Reviewer's previous remark.

- Our concern with respect to the work of Scheurich was that the size of his domain could be sufficiently small so that the clipping performed at the outflow could significantly influence the velocity field at the turbine. This was one possible explanation of the discrepancy between the velocity fields. With a longer domain and the presence of the normal outflow conditions, our simulation is more accurate in this respect.

  Withstanding the remark of the reviewer, though, other factors influencing the loading of the blade could explain the difference between the velocity fields.

Definitely, a new comparison based on a case at the same loading would be an improvement. The effect of curvature correction should also be sorted out.

Comment 8. P10, "The number of blades also has a strong influence; the two-bladed machine of Section 3.1 exhibits such vortex-blade collisions, in spite of its high loading." How does this relationship work?

The purpose of this first study was not to investigate in details the influence of the number of turbine blades. However, it is clear that it plays a major role in the geometry of the wake. To answer the Reviewer's comment, a detailed analysis of the interaction of the shed vortex sheet with the downstream blade and the different kinds of vortex interactions in this configuration should be performed.

Comment 9. P11, For the discussion about figure 6, to get a better insight into the mechanism of turbulence creation in the wake corners, would it maybe be valuable to add an impression from the side as well? Then it is easier to see what happens in the corners.

Data required to build statistics in that plane were not collected. We may only refer to 3D views to get insights into the mechanisms of turbulence creation in the wake corners: we can then refer to the discussion above on vortex reconnections and also Fig.2 of the present document.

Comment 10. P12,"The deformation of the velocity deficit clearly hints at the presence of mean streamwise vortices along the corners of the wake, a clear departure from a HAWT wake" This is only true for a HAWT subject to axial flow, but certainly not for inclined inflow for which a lateral force component is apparent (which is in practice always the case).

We totally agree with the reviewer and consider the following correction: "[...] a clear departure from a HAWT wake with no sideslip angle."

Comment 11. P12, ". . ., which makes the use of a pointwise velocity deficit unsuitable." - suggestion -Which makes the definition of a velocity deficit profile based upon a single characteristic point unsuitable.

This Reviewer's comment makes the sentence clearer. We agree with the suggestion of correction, except that we consider to adapt the term "profile" which could be misleading in that context. Therefore, the following correction will be brought: "[...] which makes the definition of a velocity deficit evolution based upon a single characteristic point unsuitable."

Comment 12. P13, The value of S1, due to continuity equation, should always be zero, except for the fact that Uinf is corrected to the local velocity outside of the wake, which is larger than Uinf. Please explain the use of S1, and its modified application.

The Reviewer's comment holds for a situation with no-through flow conditions imposed at some finite distance in the transverse directions, i.e. imposing a blockage. This would be the case for a wind tunnel test, and we agree that, in that case, S1 must asymptotically go to zero. However, in our simulations, there is a leakage flow through the boundary on the sides, which is permitted by the unbounded conditions of our velocity solver. Thus, the mass flow rate at the inflow of our simulation domain may be different from the mass flow rate at the outflow. Therefore, it is not that surprising that the value of S1 does not tend to 0 in our analyses, because of the transversal component of the velocity on the side boundaries. For the very same reason, the velocity which is recovered outside of the wake is exactly U_∞ and must not be corrected.

Finally, the authors had introduced S1 in a parallel with a displacement thickness, as a means to measure how fast the wake decays in terms of velocity deficit.

Comment 13. P13, maybe add a reference for the $x/D \sim 50$ statement? And probably a discussion about the decay laws for HAWTS, in practice these seem to deviate significantly from bluff-body flow rules in case of turbulent inflow.

References to that statement can be found in [5] (pp.151) and also in [6]. It is valid for bluff bodies, indeed. We agree that a thorough comparison with observed HAWT wake decay laws is an interesting avenue for future work. Indeed, as noted by the Reviewer, it was shown by [7] that, although the velocity deficit behind a HAWT without inflow turbulence behaves similarly to what's observed behind bluff bodies (i.e. a pointwise velocity deficit in $x^{-2/3}$), it's not the case with a turbulent inflow (where the bluff body theory would expect the pointwise velocity deficit to behave like x^{-1}).

To extend a bit our discussion on the asymptotic behavior of the wake (without going into details), we propose adding to the original text: "The decay observed for $x/D > 5$ for most of the configurations does however hint at a power-law-like behavior. For HAWTs, it has been observed that the decay deviates significantly from the bluff body behavior in the presence of a turbulence inflow [7]; similarly, it will be interesting to assess the sensitivity of VAWT wake decay with respect the turbulence intensity."

References (local numbering)

[1] D. Castelein, Dynamic stall on vertical axis wind turbines - creating a benchmark of vertical axis wind turbines in dynamic stall for validating numerical models, Master's thesis, Technische Universiteit Delft (2015).

[2] A. Bianchini, E. A. Carnevale, L. Ferrari, A model to account for the virtual camber effect in the performance prediction of an h-darrieus vawt using the momentum models, Wind Engineering 35 (4) (2011) 465–482. doi:10.1260/0309-524X.35.4.465.

[3] P. Migliore, W. Wolfe, Some effects of flow curvature on the performance of Darrieus wind turbines, American Institute of Aeronautics and Astronautics, 1979. doi:doi:10.2514/6.1979-112.

[4] L. Beaudet, Etude expérimentale et numérique du décrochage dynamique sur une éolienne à axe vertical de forte solidité, Ph.D. thesis, Université de Poitiers (2014).

[5] S. B. Pope, Turbulent flows, IOP Publishing, 2001.

[6] H. Tennekes, J. L. Lumley, A First Course in Turbulence, MIT Press, 1972.

[7] I. Litvinov, I. Naumov, V. Okulov, R. F. Mikkelsen, Comparison of far wakes behind a solid disk and a three-blade rotor, Journal of Flow Visualization and Image Processing 22 (4).

Vortex Particle-Mesh simulations of Vertical Axis Wind Turbine flows: from the airfoil performance to the very far wake

Philippe Chatelain[1], Matthieu Duponcheel[1], Denis-Gabriel Caprace[1], Yves Marichal[1,2], and Grégoire Winckelmans[1]

[1]Institute of Mechanics, Materials and Civil Engineering, Université catholique de Louvain, 1348 Louvain-la-Neuve, Belgium
[2]Wake Prediction Technologies (WaPT), Rue Louis de Geer 6, 1348 Louvain-la-Neuve, Belgium

Correspondence to: P. Chatelain (philippe.chatelain@uclouvain.be)

Abstract. A Vortex Particle-Mesh (VPM) method with immersed lifting lines has been developed and validated. Based on the vorticity-velocity formulation of the Navier-Stokes equations, it combines the advantages of a particle method and of a mesh-based approach. The immersed lifting lines handle the creation of vorticity from the blade elements and its early development. LES of Vertical Axis Wind Turbine (VAWT) flows are performed. The complex wake development is captured in details and over up to 15 diameters downstream: from the blades to the near wake coherent vortices, then through the transitional ones to the fully developed turbulent far wake (beyond 10 rotor diameters). The statistics and topology of the mean flow are studied. The computational sizes also allow insights into the detailed unsteady vortex dynamics, including some unexpected topological flow features.

1 Introduction

The aerodynamics of Vertical Axis Wind Turbines (VAWTs) are inherently unsteady, which leads to vorticity shedding mechanisms due to both the lift distribution along the blade and its time evolution. This translates into a wake topology that is far more complex and unsteady than for their Horizontal Axis counterparts (HAWTs), a characteristic which could be indicative of more intense wake decay mechanisms for VAWTs. Additionally, their inherent insensitivity to wind direction changes hints at a more robust efficiency in turbulent conditions. Logically, both traits have led to several claims of an advantage of VAWTs over HAWTs in wind farms (e.g., Paquette and Barone, 2012; Kinzel et al., 2012), and thence the promises of higher power extraction densities. Those, together with potential operational gains (maintenance costs, the disappearance of yawing actuation), have spurred some definite research momentum in VAWT aerodynamics, in the shape of experimental (Ferreira et al., 2009; Beaudet, 2014) and numerical (Scheurich, 2011; Ferreira et al., 2014) studies. However, because of their unsteady aerodynamics, VAWT simulation and modeling tools have not reached yet the level of development of those for HAWTs, e.g. the Blade Element Momentum method. Numerical investigations of VAWT wake phenomena have only been tackled recently (Scheurich and Brown, 2013) but the volume of these efforts is quite underwhelming when compared to all the comparable works on HAWTs (Sørensen et al., 2015) and the computational domains and resolutions of existing studies are quite limited. In this paper, we perform large-scale, highly-resolved Large Eddy Simulation of the flows past Vertical Axis Wind Turbines by means of a state-of-the-art Vortex Particle-Mesh (VPM) method combined with immersed lifting lines (Chatelain et al., 2013). We focus on the intrinsic vortex dynamics and wake decay mechanisms; all simulations are thus carried out without turbulence in the wind. The simulation tool is validated against experimental aerodynamic data and is then run for a standard, medium-solidity, H-shaped machine: mean flow and turbulence statistics are computed over more than 15 diameters downstream of the machine. The sensitivity of the wake behavior to the operating conditions (Tip Speed Ratio, TSR) and to the machine aspect ratio (AR) is also assessed. This paper is structured as follows. We briefly recall the Vortex Particle-Mesh (VPM) method in Section 2 and present some of the advances that enabled the Large Eddy Simulation of wind turbines within this VPM context: the multiscale Sub-Grid Scale model and the modeling of blades through immersed lifting lines. Section 3 presents some validation of our methodology, then moves to the study of a standard VAWT from the perspectives of its aerodynamics and its wake dynamics. We close this paper in Section 4 with our conclusions and perspectives.

2 Methodology

2.1 The Vortex Particle-Mesh method

The coarse scale aerodynamics and the wake of the VAWT are simulated using a massively parallel implementation of a Vortex Particle-Mesh flow solver. The present method relies on the Large Eddy Simulation in the vorticity-velocity formulation for incompressible flows ($\nabla \cdot \boldsymbol{u} = 0$)

$$\frac{D\boldsymbol{\omega}}{Dt} = (\boldsymbol{\omega} \cdot \nabla)\,\boldsymbol{u} + \nu \nabla^2 \boldsymbol{\omega} + \nabla \cdot \mathbf{T}^M \tag{1}$$

where ν is the kinematic viscosity, and $\mathbf{T}^M$ is the Sub-Grid Scale (SGS) model. The velocity field is recovered from the vorticity by solving the Poisson equation

$$\nabla^2 \boldsymbol{u} = -\nabla \times \boldsymbol{\omega}\,. \tag{2}$$

The advection of vorticity is handled in a Lagrangian fashion using particles, characterized by a position $\boldsymbol{x}_p$, a volume V_p and a vorticity integral $\boldsymbol{\alpha}_p = \int_{V_p} \boldsymbol{\omega} d\boldsymbol{x}$

$$\frac{d\boldsymbol{x}_p}{dt} = \boldsymbol{u}_p \tag{3}$$

$$\frac{d\boldsymbol{\alpha}_p}{dt} = \left((\boldsymbol{\omega} \cdot \nabla)\boldsymbol{u} + \nu \nabla^2 \boldsymbol{\omega} + \nabla \cdot \mathbf{T}^M\right)_p V_p\,, \tag{4}$$

where we identify the roles of the velocity field in the advection, and of the vortex stretching, diffusion and SGS terms for the evolution of vorticity.

The right-hand sides of these equations are evaluated efficiently on an underlying mesh (Chatelain et al., 2008). The stretching and diffusion operators use fourth-order finite differences and Eq. (2) is solved efficiently with a Fourier-based solver. In this work, we rely on the technique used by Chatelain and Koumoutsakos (2010), which handled a combination of periodic and unbounded directions through the approach of Hockney and Eastwood (1988). It is here extended to an inflow-outflow direction, say x, and two unbounded directions, y and z. A Fourier transform along x yields

$$\nabla^2_{yz}\tilde{\boldsymbol{u}} - k_x^2\tilde{\boldsymbol{u}} = -\widetilde{\nabla\times\boldsymbol{\omega}}\,, \tag{5}$$

where $\tilde{\boldsymbol{u}}(k_x, y, z)$ stands for the x-transformed field. For a given k_x mode, this is a two-dimensional Helmholtz equation in an unbounded (y,z)-domain; it is solved through a convolution with the corresponding Green's function in Fourier space through the domain-doubling technique of Hockney and Eastwood (1988), see (Chatelain and Koumoutsakos, 2010) for details. The wavenumbers k_x are here constrained to produce inflow-outflow conditions, or equivalently to only permit adequately-phased sine or cosine modes. The following conditions on the streamwise velocity are then imposed: $u_x(0,y,z) = U_\infty$ at the inflow, and $\frac{\partial u_x}{\partial x}(L_x,y,z) = 0$ at the outflow. These are completed with the conditions on the transverse components $\frac{\partial u_y}{\partial x}(0,y,z) = \frac{\partial u_z}{\partial x}(0,y,z) = 0$ and $u_y(L_x,y,z) = u_z(L_x,y,z) = 0$.

The SGS model is a simplified version of the Variational Multiscale (VM) model (Hughes et al., 2001), known as the Regularized version (RVM) (Jeanmart and Winckelmans, 2007). In that variant, the SGS model is designed as an eddy viscosity model acting only on the small scale field

$$\mathbf{T}^M = \nu_{SGS}\left(\nabla\boldsymbol{\omega}^s + \nabla^t\boldsymbol{\omega}^s\right) \tag{6}$$

where $\boldsymbol{\omega}^s$ represents the small-scales part of the vorticity field obtained by high-pass filtering. The eddy viscosity is taken as $\nu_{SGS} = C_r^{(n)}\Delta^2\left(2\mathbf{S}:\mathbf{S}\right)^{1/2}$ where the strain rate $\mathbf{S}$ is evaluated using the complete velocity field. We refer to Cocle et al. (2007, 2008, 2009) for implementation details and for the values of the coefficients $C_r^{(n)}$ when using filtering of order $2n$.

In order to carry out the computational steps above, information is made available on the mesh, and recuperated from the mesh, by interpolating back and forth between the particles and the grid using high order interpolation schemes. Advantageously, this hybridization does not affect the good numerical accuracy (in terms of diffusion and dispersion errors) and the stability properties of a particle method. The present method indeed still waives the typical CFL constraint for the explicit time integration of advection, $\Delta t < C_u h/\|\boldsymbol{u}\|_{\max}$, and rather involves higher order constraints (Koumoutsakos, 2005), e.g. $\Delta t < C_{\nabla u}/\|\nabla\boldsymbol{u}\|_{\max}$; this essentially corresponds to preventing particle trajectories from crossing each other. The time integration scheme used in the present work is a low-storage third order Runge-Kutta (Williamson, 1980).

This last discussion actually pertains to the issue of Lagrangian distortion in particle methods. If left alone, particles can be seen to deplete regions of the flow or cluster in others. Several remedies have been proposed. Dissipative terms can be added to the particle ODEs in order to limit the particle deformations (Monaghan, 2000); this comes at the price of artificial bulk and shear viscosities. State-of-the-art particle methods, such as the present one, rely on a procedure called remeshing (Cottet, 1996; Koumoutsakos, 1997; Ploumhans and Winckelmans, 2000; Winckelmans, 2004), which consists in the periodic regularization of the particle set onto a mesh. This procedure typically relies on high order interpolation formulas (Monaghan, 1985; van Rees et al., 2011) which do involve well controlled levels of artificial viscosity. All the simulations of Section 3 have involved a remeshing operation every 5 time steps that uses the third order accurate M_4' scheme of Monaghan (1985); the same scheme is used for the particle-to-mesh and mesh-to-particle interpolation operations.

2.2 Immersed lifting lines

The generation of vorticity along the blades is accounted for through an immersed lifting line approach (Chatelain et al., 2013). The approach is very much akin to a Vortex Lattice method and relies on the Kutta-Joukowski theorem (see e.g. (Prandtl, 1923)) that relates the developed lift $\boldsymbol{L}$ to the relative flow $\boldsymbol{V}_{\text{rel}}$ and the circulation bound around the local 2D airfoil

$$\boldsymbol{L} = \rho \boldsymbol{V}_{\text{rel}} \times \boldsymbol{\Gamma}\,. \tag{7}$$

Lift can also be obtained from the relative flow, its angle of attack α and the airfoil lift coefficient $C_l(\alpha)$; equating this aerodynamics-provided expression to Eq. (7) allows to solve for the instantaneous circulation $\boldsymbol{\Gamma}$ at a blade location. The solenoidal property of vorticity then imposes that streamwise and spanwise vorticities be shed from the lifting line in order to account for spanwise and temporal variations of $\boldsymbol{\Gamma}$, respectively. Over a time step, the shed vorticity is constructed thanks to Lagrangian tracers released along the blade. The vorticity bound to the blade and the newly generated vorticity are discretized by means of particles immersed in the mesh and in the bulk flow-representing particles; their treatment thus fits within the present particle-mesh framework. Unlike the mesh-only Vorticity Transport Model (Brown and Line, 2002) or an Actuator Line technique (Sørensen et al., 2015), this treatment of vorticity sources is Lagrangian and well suited for the large time steps enabled by the rest of the method. The aerodynamic behavior of the lifting lines sections, i.e. C_l and $\boldsymbol{\Gamma}$, account for unsteady effects through a Leishman-Beddoes dynamic stall model (Leishman, 2006). This semi-empirical model shows a good trade-off between simplicity and accuracy, provided that the model coefficients are validated with relevant experimental data. In this work, we follow the indications of Dyachuk (Dyachuk et al., 2014) and Scheurich (Scheurich, 2011) who present coefficients for various airfoils validated in the particular case of a VAWT.

The standard lifting line and the actuator line techniques are not able to capture flow curvature effects. Indeed, if the flow relative to the blade is curved, as it is the case here for a blade in rotation through essentially straight streamlines, the airfoil behaves as an airfoil with an additional camber Migliore and Wolfe (1979); Beaudet (2014). We consider a blade with a chord c tangentially positioned at a radius R for its quarter-chord position, this additional camber can be modeled in a straightforward manner by pitching the blade inwards by an angle $\alpha_0 = \arctan\left((1-\cos(\beta/2))/\sin(\beta/2)\right)$ where $\beta = \arctan(c/2\,R) + \arctan(c/2\,R)$. In the validation section below (Sec 3.1), we verify the positive effect of such a correction. Finally, we note that these methods (Immersed lifting line or actuator line) in their standard versions do not capture the internal turbulent fluctuations of the actually shed structures.

3 Results

3.1 Validation

We first present validation results against recent work (Castelein, 2015) for a low solidity two-bladed H-shaped machine with NACA0018 airfoils. The parameters for the Leishman-Beddoes dynamic stall model are based on those for a NACA0015 in (Scheurich, 2011); they are here tuned to fit the static behavior of the polar at the Reynolds number of the experiment at

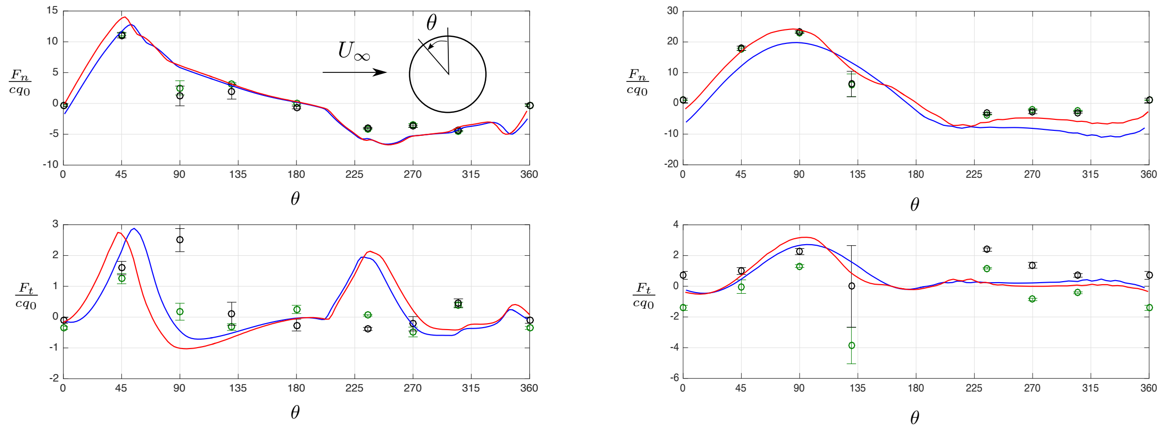

(a) TSR $= 2.0$ (b) TSR $= 4.5$

Figure 1. Validation: evolution of the normal, $F_n/(c\,q_0)$, and tangential, $F_t/(c\,q_0)$, force coefficients at mid-height vs the blade angular position θ; VPM simulation without curvature correction (blue solid line) and with curvature correction (red solid line), experimental results (o) with two techniques of force computation from PIV flow fields (Castelein, 2015).

the design point, $Re = U_{\mathrm{rel}}c/\nu = 1.5\,10^5$. Throughout this paper, we use the following axes convention: x is the streamwise direction, y is cross-stream and orthogonal to the VAWT axis, which z is parallel to. The origin for the blade angular position θ is set at the upwind-going position. Figure 1 presents the profiles of the normal and tangential forces developed by a blade over a revolution, non-dimensionalized with respect to the profile chord c and the dynamic pressure $q_0 = 1/2\,\rho U_\infty^2$. We report on VPM simulations with and without a curvature correction, which here amounts to a inward pitch $\alpha_0 = 1.72°$. This correction appears to bring a notable improvement of the results particularly for the moderate TSR $= \Omega\,R/U_\infty$: the explored angles of attack are indeed smaller than at low TSR. While the results at an intermediate TSR show good agreement (Fig. 1(b)), there is a clear departure at the lower TSR (Fig. 1(a)). The experimental points hint at a stall happening later on the upstream stretch, around $90°$, and more abruptly than for the simulation; we report here that the authors of the experiment advised to use circumspection for the F_n data at $135°$ and clearly question the validity of their results for F_t through the whole rotation. We nevertheless confront our simulations to all their results in Fig. 1. This mismatch on the upstream part has a direct influence on the predictions for the downstream stretch ($\theta \in [210°, 270°]$), as the stall-generated structures are advected through the rotor; this may explain the marked differences observed there. These results are satisfactory: they are indeed very sensitive to the dynamic stall model, here probably still misadapted, and to some unquantified uncertainties for the experimental facility (the TU Delft Open Jet Wind Tunnel), namely its blockage and secondary flows in the test section.

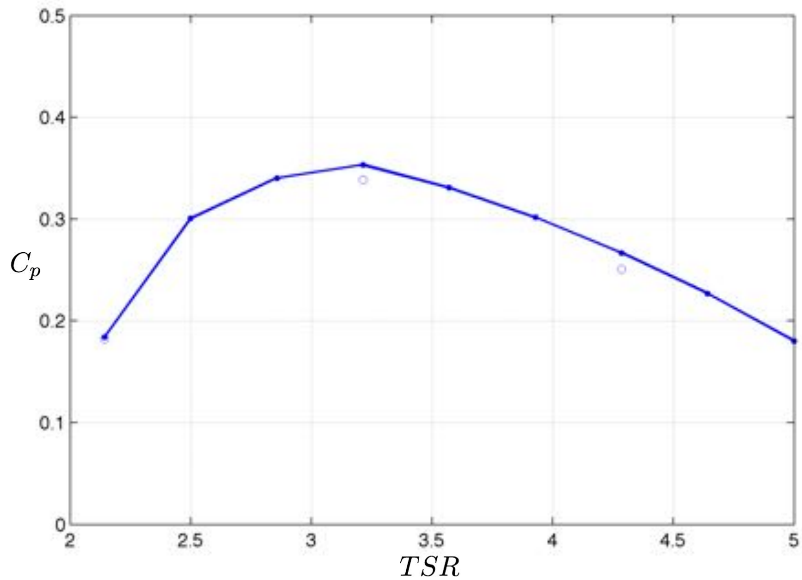

Figure 2. H-type VAWT with $AR = 1.5$: power coefficient curve obtained at intermediate resolution ($D/h = 48$, solid line) and configurations investigated at high resolution ($D/h = 96$, circles).

3.2 Aerodynamics

The remainder of this section focuses on a low solidity H-VAWT studied numerically by Scheurich et al. (2010); Scheurich (2011). For the sake of completeness, we here briefly recall its main parameters: an aspect ratio $AR = H/D = 1.5$, a solidity $\sigma = nc/D = 0.1725$, and constant-chord NACA0015 airfoils. Simulations were run without the curvature correction investigated above (or equivalently, the simulated corresponds to a machine with a blade pitched outwards by $\alpha_0 = 1.65°$).

Figure 2 shows this machine's power coefficient (C_p) curve as a function of the TSR. In order to be computationally affordable, the whole curve has been produced using an intermediate resolution of $D/h = 48$ mesh points/particles per diameter; it allows to identify the optimum power operating point at TSR $= 3.21$. We investigate the behaviors of the aerodynamics and wake topology of this baseline point, two off-design points (TSR $= 2.14$, 4.28), and also different aspect ratios $AR = 1.0$, 3.0. These configurations have been simulated at a fine resolution $D/h = 96$ and in domains that extended up to 17 diameters downstream of the rotor axis.

Figure 3 presents the aerodynamic behavior at mid-height. A lower resolution result ($D/h = 48$) is also shown for the baseline TSR and demonstrates the converged state of our simulations. The aspect ratio only affects marginally the aerodynamics in the middle of the blades; its effects will be discussed further below. A positive angle of attack corresponds to a relative velocity coming from outside of the cylinder swept by the blades. The angle of attack evolution during a revolution is not symmetrical for the upstream and downstream legs because of the reduced velocity encountered downstream. At the baseline

TSR, it reaches a maximum just after the most upstream position ($15°$ around $\theta = 120°$) and the downstream region is characterized by a plateau close to $-7°$. Also of note are the oscillations around $210°$ and $330°$, in the angle of attack and the force coefficients. These are quite well-resolved and physical: as discussed in Section 3.3, the vortex sheets shed during the upstream leg indeed impinge upon the blade in its downstream leg; the velocity jumps associated with these sheets then cause variations in the velocity relative to the blade. The off-design operating points exhibit the expected behaviors: a high TSR will lead to

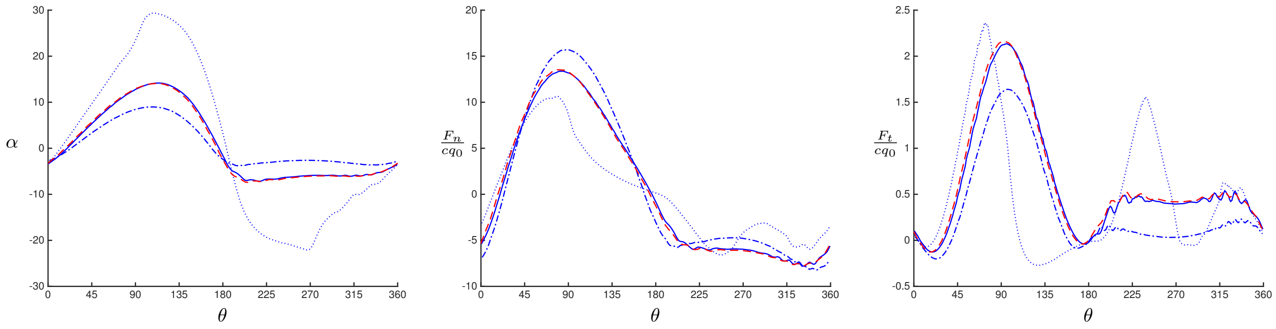

(a) Angle of attack (b) Normal force coefficient (c) Tangential force coefficient

Figure 3. H-type VAWT with $AR = 1.5$: evolution of the angle of attack and of the normal, $F_n/(cq_0)$, and tangential, $F_t/(cq_0)$, force coefficients at mid-span versus the blade angular position θ at $TSR = 2.14$ (dotted), 3.21 (solid), and 4.28 (dash-dotted); an intermediate resolution ($D/h = 48$) result for $TSR = 3.21$ is also shown (dash).

smaller angles of attack and a decreased torque production while the low TSR causes a distinctive stall in the upstream region and also in the downstream one. It is visible in the sharp transitions of the force coefficients at $90°$ and $270°$. The AoA exhibits different behaviors, but consistent with the physics. In the upstream region, the flow is dominated by the blockage effect: as the loading decreases because of stall, the AoA increases even faster; downstream, the blade initially sees a flow less impacted by the stalled upstream part but then encounters the wake of the unstalled part ($\theta \in [0°, 90°]$) and drops rapidly ($\theta = 270°$). Finally, we summarize the effects of TSR, AR and simulation resolution on the estimation of global performance figures in Table 1. As expected, the power, thrust and sideforce coefficients are quite sensitive to the TSR. The machine aspect ratio, however, does not seem to have a major impact on them: going from $AR = 1$ to 3 only improves the C_P by less than 2%.

3.3 Wakes

3.3.1 Vortex dynamics

The instantaneous wakes of the $AR = 1.5$ machine at the three considered TSRs are visualized through volume rendering of the vorticity magnitude in Fig. 4. They allow several insights into the complex vortical structure of the wake which is significantly different from that of a HAWT. We first consider the design TSR (Fig. 4(b)). The vorticity shed in the wake consists in (i) the blade tip vortices, which constitute the top and bottom sides of the wake, and (ii) the vortex sheets, shed due to the time-

Table 1. H-VAWT global performance: effects of aspect ratio, TSR and spatial resolution.

AR	TSR	C_P		C_x		C_y	
	D/h	48	96	48	96	48	96
1.0	3.21		0.338		0.844		0.0344
1.5	2.14	0.184	0.182	0.556	0.557	−0.0518	−0.0376
1.5	3.21	0.353	0.339	0.863	0.845	0.0193	0.0435
1.5	4.28	0.267	0.250	0.910	0.887	0.0390	0.0683
3.0	3.21		0.344		0.852		0.0616

variation of the circulation of the blades, which form the lateral sides. The tip vortices are the strongest in the vicinity of the upstream- and downstream-most positions of the blades (around $\theta = 90°$ and $270°$) where the blades operate at their maximum angle of attack. There, depending on the appearance of stall, or delayed stall effects, the blade will achieve its maximum circulation then lose it either abruptly or progressively, depending on whether the blade is stalled or not. At the design TSR, the blade exploits the delayed stall at its most: its circulation keeps increasing, well past $\theta = 90°$, and then smoothly decreases. This is explained by two phenomena: (1) the airfoil experiences the highest delay in the circulation development (beneficial in this case as it widens the extent of torque production by the blade); (2) the leading edge vortex does not introduce a sharp drop in circulation yet (which clearly happens at lower TSR, see Fig.3b). The $d\Gamma/dt$ vorticity shedding is maximum when the blades are close to their lateral positions $\theta = 0°$ (upwind leg) and $180°$ (downwind leg). The corners of the wake, i.e. the intersections of the two types of vortical structures described above, give rise to the fastest-growing vortical instabilities which quickly propagate and cause the pairing of vortices of unequal circulations. Indeed, the unsteady aerodynamics have produced vortices with a varying circulation and the shed vortices will interact with a different section of a preceding/succeeding vortex. In this kind of event, the stronger vortex distorts the weaker one, leading to intense stretching, enstrophy production, and the propagation of disturbances along the vortex cores therefore bringing an overwhelming contribution to the transition to turbulence. This mechanism, most visible in Fig. 4(a) and isolated in Fig. 5, is well known in vortex dynamics and had already been identified on aircraft wakes (Bristol et al., 2004; Leweke et al., 2016). As a direct consequence, the turbulent regions of the wake grow from the corners and the wake only reaches a fully turbulent state once these regions have merged: the distance to reach this state will be governed directly by the aspect ratio of the machine.

The VAWT wake decay is of course also governed by the TSR in a fashion very similar to that of the HAWT: a high TSR (Fig. 4(c)) induces narrower vortex separations, which directly condition the growth rate of the instabilities and the time to the reconnection events. This directly, and very geometrically, translates in an increasing opening angle for the envelopes of the corner vortical structures, going from Fig. 4(a) to 4(c)). Decreasing the TSR below the design point actually affects the wake even more dramatically. The stall event on the upstream part of the revolution weakens the upstream wake contribution

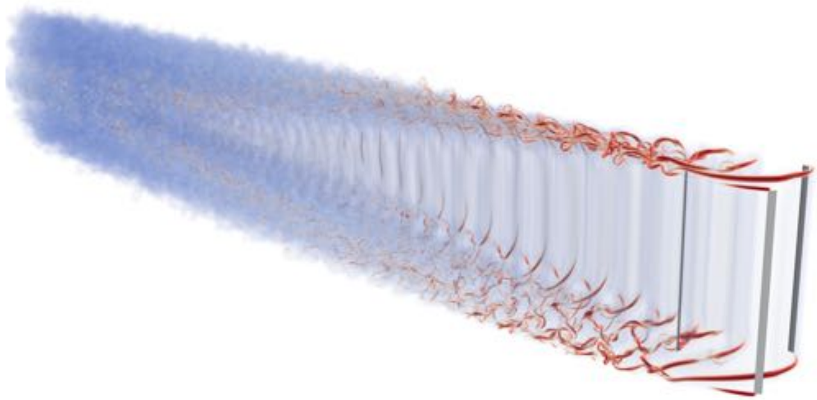

(a) $\mathrm{TSR} = 2.14$

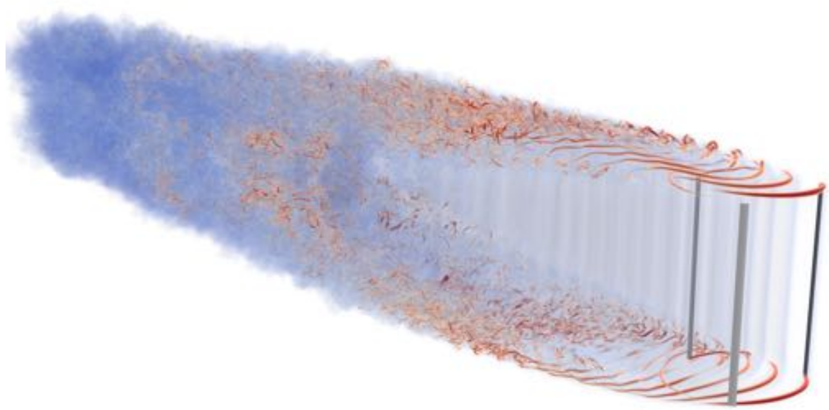

(b) $\mathrm{TSR} = 3.21$

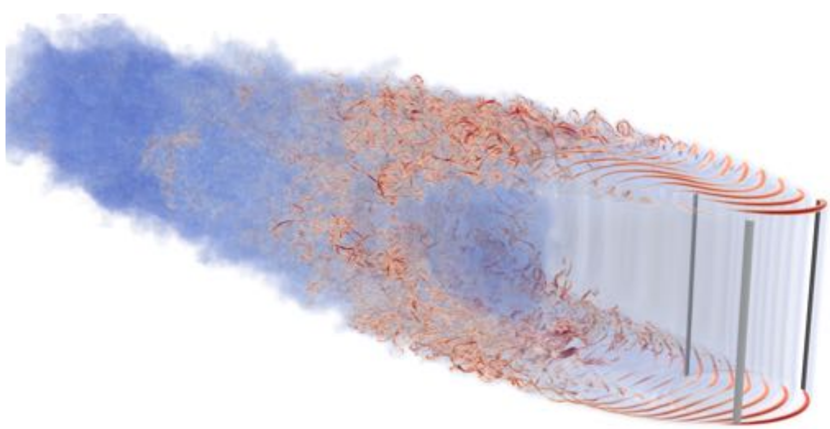

(c) $\mathrm{TSR} = 4.28$

Figure 4. H-type VAWT with $AR = 1.5$: volume rendering of the vorticity magnitude $\|\boldsymbol{\omega}\|$; the lifting lines are also shown as 3-D blades.

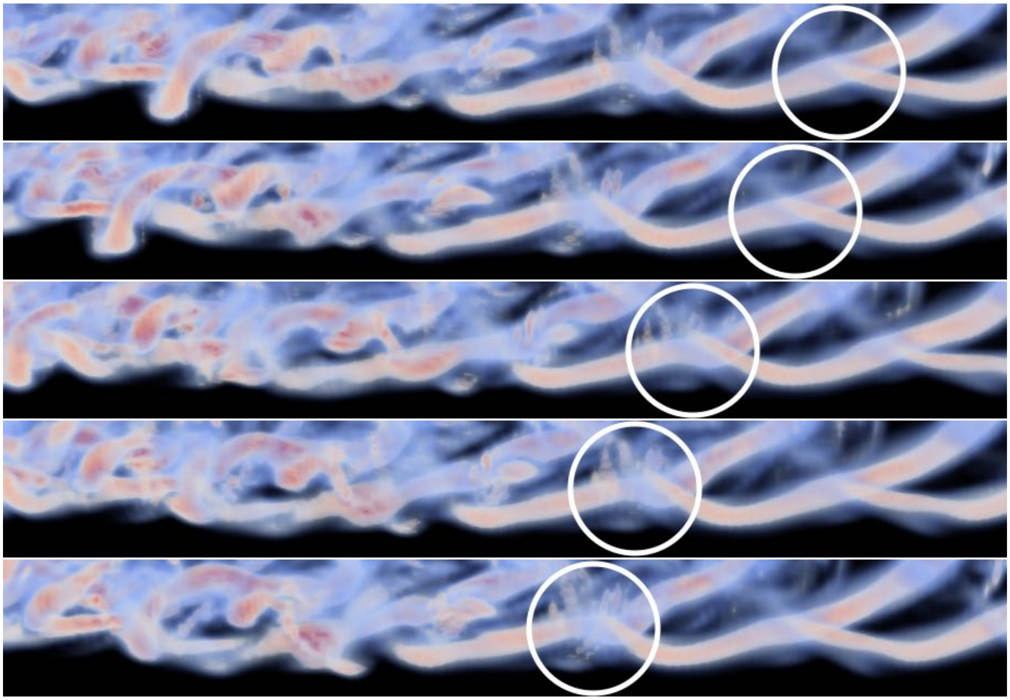

Figure 5. H-type VAWT with $AR = 1.5$: volume rendering of the vorticity magnitude $||\boldsymbol{\omega}||$; vortex reconnections are visible on the side of the wake, here illustrated in the area behind the bottom left corner of the VAWT, at successive times. The turbine is on the right, and the velocity is directed to the left.

(between $\theta = 90°$ and $180°$), generating a stopping vortex that will be advected through the rotor (Fig. 4(a)). One can thus expect a two-lobed wake. Conversely, higher TSRs exhibit weaker vortical structures being advected through the rotor. As discussed in Section 3.2, the $d\Gamma/dt$ sheets shed on the upstream leg will cross the rotor and impact the blade aerodynamics on the downstream leg, with an extreme case being the above-discussed stall event.

The behaviors of the upstream tip vortices within the rotor are more complex to apprehend, as they are affected by several factors: the intrinsic roll-up dynamics of a vortex sheet (with a time-varying strength) and the velocities induced by the surrounding vortical structures, including the bound vortices on the blades. To some degree, the latter can be crudely linked to the overall rotor loading (the C_x values of Table 1). For a highly loaded rotor (TSR $= 3.21$ and 4.28), the generated blockage effects will push the vortices shed upstream vertically and away from the downstream blade tips. One only sees the upstream tip vortices impinging upon the downstream blades at a low rotor loading, as it is the case for TSR $= 2.14$. This observation does not agree with the results of Scheurich and Brown (Scheurich and Brown, 2013), which showed upstream vortices colliding the blades at high TSRs. A possible explanation might lie in the relatively short domain and the direct use of the unbounded Biot-Savart law in their work. One needs to add additional terms to enforce an outflow condition for this otherwise clipped vorticity field; the present study does precisely that by enforcing a normal outflow velocity ($\partial u/\partial x = 0$, $v = 0$, $w = 0$) through

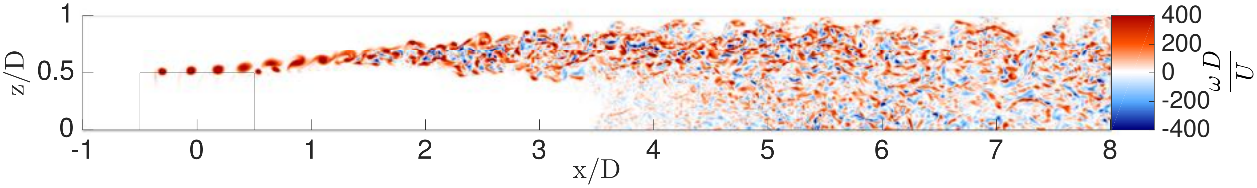

(a) $\mathrm{AR} = 1.0$

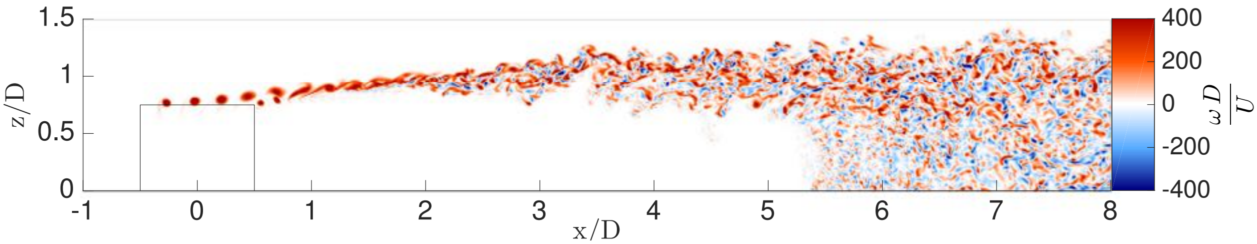

(b) $\mathrm{AR} = 1.5$

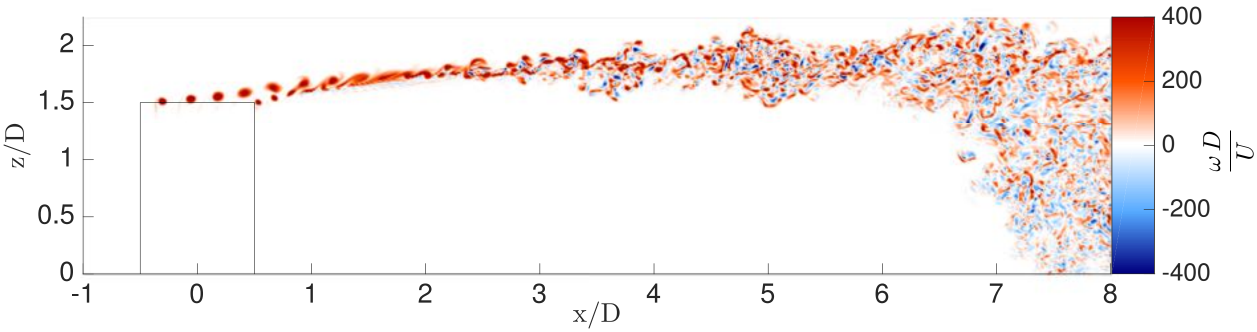

(c) $\mathrm{AR} = 3.0$

Figure 6. Effect of aspect ratio at $\mathrm{TSR} = 3.21$: contours of the instantaneous cross-stream vorticity component $\omega_y D/U_\infty$.

its Fourier-based solver (Chatelain and Koumoutsakos, 2010). Other explanations could also be found in a mismatch in the achieved loading by the VAWT and the use of a curvature correction; these effects should be further investigated.

Blockage is but one, and global, factor however. The discussion can be refined as additional, and less immediate, effects are to be expected from the machine geometry. The aspect ratio, as indicated by C_x in Table 1, has a small effect on the blockage and one can also expect an influence on the 3D topology of this blockage effect: a higher AR thus leads to an increased clearance between the vortices and the blade, as shown in Fig. 6. The number of blades also has a strong influence; the two-bladed machine of Section 3.1 (not shown here, also see (He, 2013)) exhibits such vortex-blade collisions, in spite of its high loading $C_x = 0.874$. Finally, beyond the rotor, the instantaneous vorticity fields of Fig. 6 also offer some insights into the pairing phenomenon of the tip vortices, the generation of a turbulent wake and the recirculation region.

3.3.2 Average flow statistics

The average behavior of these wakes is studied through the mean axial velocity $\bar{u}$ and the turbulent kinetic energy $\bar{k}$; these statistics were collected over a period $T_{\text{avg}} = 30\,D/U_\infty$. Figure 7 shows a horizontal slice of these statistics for the $AR = 1.5$ machine. This averaged wake exhibits several prominent features that reflect the phenomena identified in the discussion above. In all the conditions, we observe the generation of TKE on the sides of the wake and the associated smearing of the velocity deficit. This is consistent with our discussion of the vortical instabilities in the corner structures and the subsequent propagation of the turbulent regions. At low TSR, the averaged velocity field does exhibit the expected two-lobed structure, with a stronger deficit on the blade-travelling-upwind side of the rotor ($\theta \in [270°, 90°]$). For the higher TSRs (Figs. 7(b) and 7(c)), a backflow region lies inside the wake at a position that varies with the TSR: it is centered at $x/D \simeq 5.5$ for $TSR = 3.21$ and at $x/D \simeq 4$ for $TSR = 4.28$. The location of this feature clearly coincides with the production of TKE and an accelerated smearing of the wake velocity deficit; this too agrees with our vortex dynamics discussion. The topology of the associated recirculation bubbles is clearly three-dimensional and will not be discussed here.

Finally, the averaged wakes exhibit a slight deviation in this mid-plane. As expected, the behaviors of the three TSRs do correlate with the signs and values of the side-forces produced by the rotor (see C_y in Table 1). These side-forces also appear in the average behavior as observed in cross-flow slices (Fig. 8). The deformation of the velocity deficit clearly hints at the presence of mean streamwise vortices along the corners of the wake (Figs. 8(a) and 8(b)), a clear departure from a HAWT wake with no side slip angle.

The mean streamwise vorticity at three transverse slices is shown in Fig. 9. Even though the statistics are converged, the near-perfect periodicity of the flow leads to a pattern of positive and negative patches, signatures of the advection of tip vortices shed on the upstream and downstream parts of the rotation, respectively. The dominant streamwise vorticity is thus difficult to identify in the near-wake but large scale structures can be identified further downstream, also thanks to the induced deformation of the wake.

3.3.3 Decay diagnostics

We apply classical turbulent wake diagnostics to the characterization of the wake decay. More specifically, we adapt integral quantities, such as the displacement and momentum widths, to the present context; the wakes being considered indeed lack symmetry and exhibit strong secondary flow structures, which makes the definition of a velocity deficit evolution based upon a single characteristic point unsuitable. Thus we define dimensionless displacement and momentum surfaces, respectively as

$$S_1(x) = \frac{1}{H\,D} \int_{-\infty}^{\infty} \int_{-\infty}^{\infty} \left(1 - \frac{u_x(x,y,z)}{U_\infty}\right) dy\,dz \tag{8}$$

$$S_2(x) = \frac{2}{H\,D} \int_{-\infty}^{\infty} \int_{-\infty}^{\infty} \left(1 - \frac{u_x(x,y,z)}{U_\infty}\right) \left(\frac{u_x(x,y,z)}{U_\infty}\right) dy\,dz\,. \tag{9}$$

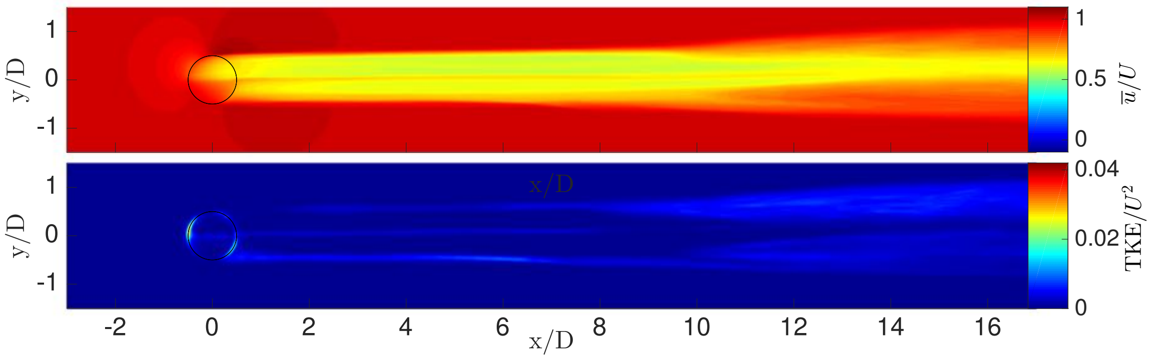

(a) TSR $= 2.14$

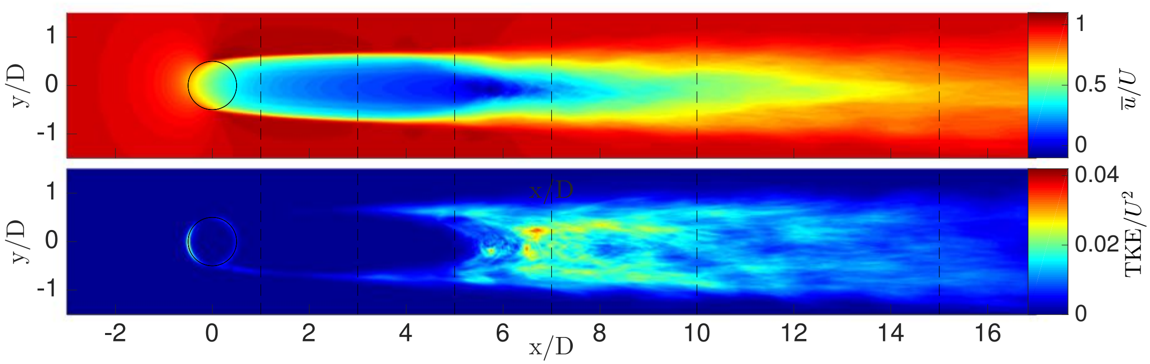

(b) TSR $= 3.21$

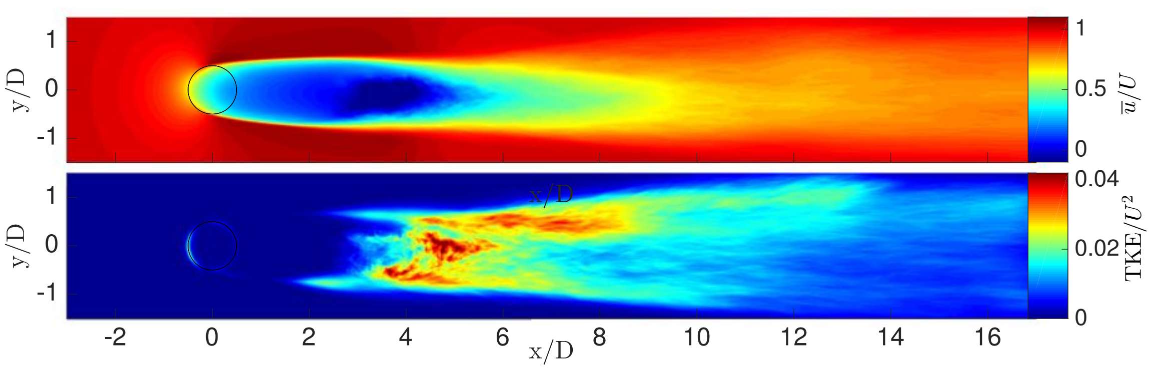

(c) TSR $= 4.28$

Figure 7. H-type VAWT with $AR = 1.5$: mean streamwise velocity $\bar{u}/U_\infty$ and resolved turbulent kinetic energy $\bar{k} = \frac{\overline{u'u'}+\overline{v'v'}+\overline{w'w'}}{2U_\infty^2}$ in the $y/D = 0$ plane.

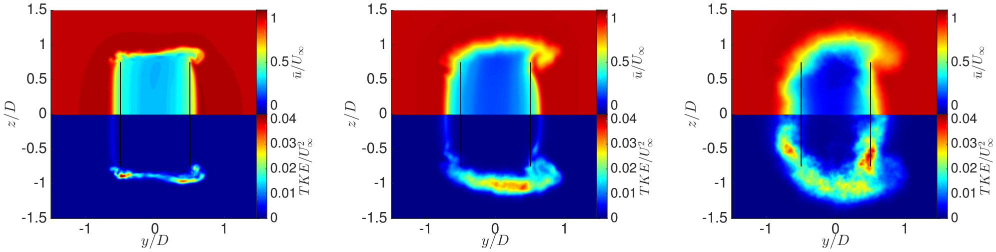

(a) $x/D = 1$ (b) $x/D = 3$ (c) $x/D = 5$

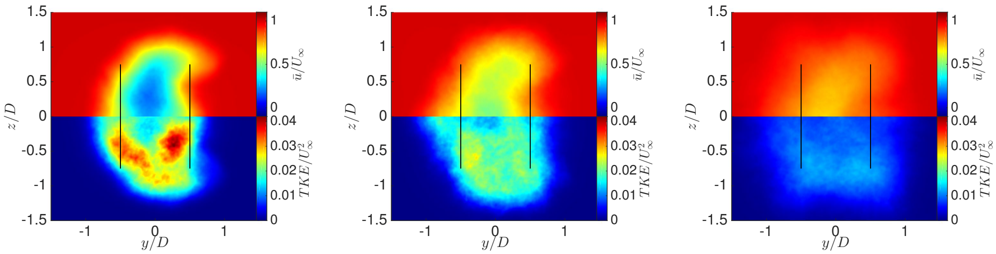

(d) $x/D = 7$ (e) $x/D = 10$ (f) $x/D = 15$

Figure 8. H-type VAWT with $AR = 1.5$: mean streamwise velocity $\bar{u}/U_\infty$ and turbulent kinetic energy $\bar{k}$ in cross-flow slices.

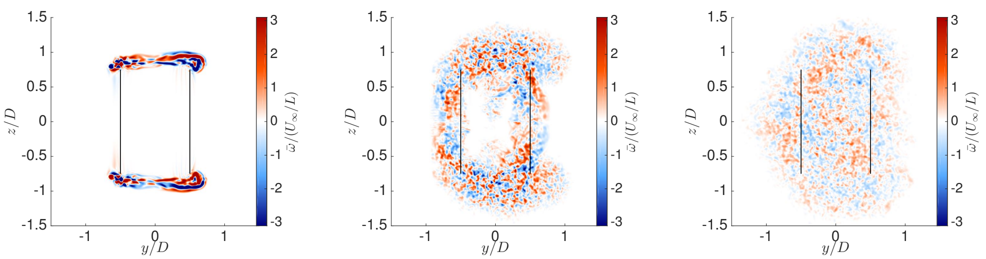

(a) $x/D = 1$ (b) $x/D = 5$ (c) $x/D = 10$

Figure 9. H-type VAWT with $AR = 1.5$: mean streamwise vorticity $\bar{\omega}/(U_\infty/L)$.

These diagnostics correspond to integrals of flux quantities in cross-stream sections located at a distance x downstream of the turbine axis. S_1 quantifies the blockage effect caused by the wake on the flow; it is shown in Fig. 10(a). As a reference, S_1 should be compared with the square of the displacement width (δ^2) of an axisymmetric wake for which classical similarity theory (Tennekes and Lumley, 1972) predicts a behavior $S_1 \sim x^{-1/3}$ in the far wake. The asymmetry of the wake generator and its proximity are such that we cannot observe the self-similarity region: classical results for bluff bodies indicate a development distance of $x/D \sim 50$ to obtain the theoretical far wake self-similarity (Pope, 2001). The decay observed for $x/D > 5$ for most of the configurations does however hint at a power-law-like behavior. For HAWTs, it has been observed that the decay deviates significantly from the bluff body behavior in the presence of a turbulence inflow (Litvinov et al., 2015); similarly, it will be interesting to assess the sensitivity of VAWT wake decay with respect the turbulence intensity. Still, the evolution of S_1 does provide a signature of the recirculation region: the magnitude and the extent of the overshoot $S_1 > 1$ correlates with the location and the size of the recirculation bubble for the design and high TSRs (Figs. 7(b) and 7(c)). This correspondence also agrees with the effect of the aspect ratio: an increasing AR pushes both the recirculation (indicated by the merging of vortical structures in the center of the wake in Fig. 6) and the S_1 overshoot further downstream.

The dimensionless momentum surface S_2 is related to the deficit in the flux of momentum in these planes. In the absence of secondary flows and pressure gradients, it should in fact correspond to the thrust coefficient $S_2 \simeq C_x$ at large distances behind the VAWT when a factor 2 is used in the definition of S_2, as here in Eq. (9). This is confirmed by our results of Fig. 10(b)): after a transition, the curves tend towards the corresponding C_x values of Table 1.

Finally, the case TSR $= 2.14$ constitutes an outlier in the discussions above. This is not unexpected: the instability growth is slower than for the other cases and does not allow the transition to a well-mixed fully-turbulent wake within the computational domain.

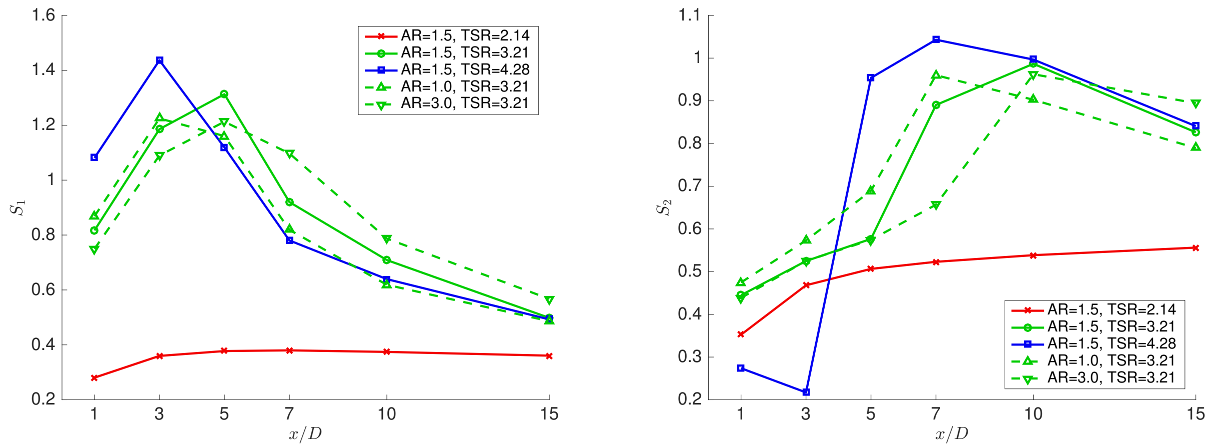

(a) Dimensionless displacement surface S_1

(b) Dimensionless momentum surface S_2

Figure 10. H-type VAWT: dimensionless displacement and momentum surfaces as functions of the streamwise coordinate.

4 Conclusions

A Vortex Particle-Mesh method, here briefly presented, has been applied to large scale and high resolution LES of VAWT wakes. The method is capable of tracking vortical structures over very long times and distances. This has led to several insights into the vortex dynamics at work inside the wakes of VAWTs. The mean flow topology has been extracted; unsteady flow aspects, three-dimensional effects and classical wake diagnostics have also been studied. The impact of several of these flow features for the deployment of VAWTs in wind farms is considerable: the aspect ratio and the operating conditions of the machine greatly affect the wake decay, and even allow the presence of a recirculation region. The present study merely constitutes a preliminary study of VAWT wakes. Direct follow-up work will investigate the 3D topology of the averaged wake and its unsteadiness. We will then also consider the behavior of these machines and of their wakes in a turbulent wind. Our methodology can also accommodate rotor dynamics models and realistic controllers; this will bring definitive answers to the smoothness of torque generation for H-type VAWTs and their performances in wind farms.

5 Code availability

The Immersed Lifting Line VPM code and its Fourier-based solver library are proprietary. The Parallel Particle-Mesh (PPM) library is an open source library (ETHZ/CSE Lab, 2011).

6 Data availability

The data sets involved in this study consist of massive 3D and time-dependent data sets, the handling of which is not tractable on a data registry.

Author contributions. P. Chatelain and M. Duponcheel prepared and ran the simulations and D.-G. Caprace performed their post-processing. P. Chatelain and M. Duponcheel developed the code; Y. Marichal and D.G. Caprace developed the dynamic stall model inside the code. P. Chatelain, M. Duponcheel and G. Winckelmans contributed to the analysis and the discussion of the results. P. Chatelain prepared the manuscript with contributions from all co-authors.

Competing interests. The authors declare that they have no conflict of interest.

Acknowledgements. The authors acknowledge the fruitful discussions with Thierry Maeder, Stefan Kern and Dominic von Terzi, at the Aerodynamics and Acoustic Lab at GE Global Research, Garching bei München. Matthieu Duponcheel was partially supported by the ENGIE-funded research project *Small Wind Turbines*. The development work benefited from the computational resources provided by the supercomputing facilities of the Université catholique de Louvain (CISM/UCL) and the Consortium des Équipements de Calcul Intensif (CÉCI) en Fédération Wallonie Bruxelles (FWB) funded by the Fond de la Recherche Scientifique de Belgique (F.R.S.-FNRS) under Convention No. 2.5020.11. The production simulations used computational resources made available on the Tier-1 supercomputer of the FWB, infrastructure funded by the Walloon Region under the Grant Agreement No. 1117545.

References

Beaudet, L.: Etude expérimentale et numérique du décrochage dynamique sur une éolienne à axe vertical de forte solidité, Ph.D. thesis, Université de Poitiers, 2014.

Bristol, R. L., Ortega, J. M., Marcus, P. S., and Savas, O.: On cooperative instabilities of parallel vortex pairs, Journal of Fluid Mechanics, 517, 331–358, 2004.

Brown, R. E. and Line, A.: Efficient High-Resolution Wake Modeling Using the Vorticity Transport Equation, AIAA Journal, 43, 1434–1443, 2002.

Castelein, D.: Dynamic stall on vertical Axis Wind Turbines - Creating a benchmark of Vertical Axis Wind Turbines in Dynamic Stall for validating numerical models, Master's thesis, Technische Universiteit Delft, 2015.

Chatelain, P. and Koumoutsakos, P.: A Fourier-based elliptic solver for vortical flows with periodic and unbounded directions, Journal of Computational Physics, 229, 2425–2431, http://www.sciencedirect.com/science/article/B6WHY-4Y4R4GD-1/2/1cf355678ffad889ad409f181e47840d, 2010.

Chatelain, P., Curioni, A., Bergdorf, M., Rossinelli, D., Andreoni, W., and Koumoutsakos, P.: Billion vortex particle Direct Numerical Simulations of aircraft wakes, Computer Methods in Applied Mechanics and Engineering, 197, 1296–1304, 2008.

Chatelain, P., Backaert, S., Winckelmans, G., and Kern, S.: Large Eddy Simulation of wind turbine wakes, in: Proceedings of The 9th International Symposium on Engineering Turbulence Modelling and Measurements (ETMM-9), June 6–8, 2012, Thessaloniki, Greece, edited by Rodi, W., vol. 91 of *Flow, Turbulence and Combustion*, pp. 587–605, ERCOFTAC, Springer, doi:10.1007/s10494-013-9474-8, 2013.

Cocle, R., Dufresne, L., and Winckelmans, G.: Investigation of multiscale subgrid models for LES of instabilities and turbulence in wake vortex systems, Lecture Notes in Computational Science and Engineering, 56, 141–159, 2007.

Cocle, R., Winckelmans, G., and Daeninck, G.: Combining the vortex-in-cell and parallel fast multipole methods for efficient domain decomposition simulations, Journal of Computational Physics, 227, 9091–9120, doi:10.1016/j.jcp.2007.10.010, 2008.

Cocle, R., Bricteux, L., and Winckelmans, G.: Scale dependence and asymptotic very high Reynolds number spectral behavior of multiscale subgrid models, Physics of Fluids, 21, 085 101, doi:10.1063/1.3194302, 2009.

Cottet, G.-H.: Artificial viscosity models for vortex and particle methods, J. Comput. Phys., 127, 299–308, 1996.

Dyachuk, E., Goude, A., and Bernhoff, H.: Dynamic stall modeling for the conditions of vertical axis wind turbines, AIAA journal, 52, 72–81, 2014.

ETHZ/CSE Lab: http://www.ppm-library.org, 2011.

Ferreira, C. S., van Kuik, G., van Bussel, G., and Scarano, F.: Visualization by PIV of dynamic stall on a vertical axis wind turbine, Experiments in Fluids, 46, 97–108, doi:10.1007/s00348-008-0543-z, http://dx.doi.org/10.1007/s00348-008-0543-z, 2009.

Ferreira, C. S., Madsen, H. A., Barone, M., Roscher, B., Deglaire, P., and Arduin, I.: Comparison of aerodynamic models for Vertical Axis Wind Turbines, Journal of Physics: Conference Series, 524, 012 125, http://stacks.iop.org/1742-6596/524/i=1/a=012125, 2014.

He, C.: Wake Dynamics Study of an H-type Vertical Axis Wind Turbine, Master's thesis, Technische Universiteit Delft, 2013.

Hockney, R. and Eastwood, J.: Computer Simulation using Particles, Taylor & Francis, Inc. Bristol, PA, USA, 1988.

Hughes, T. J. R., Mazzei, L., Oberai, A. A., and Wray, A. A.: The multiscale formulation of large eddy simulation: Decay of homogeneous isotropic turbulence, Physics of Fluids, 13, 505–512, doi:http://dx.doi.org/10.1063/1.1332391, http://scitation.aip.org/content/aip/journal/pof2/13/2/10.1063/1.1332391, 2001.

Jeanmart, H. and Winckelmans, G.: Investigation of eddy-viscosity models modified using discrete filters: A simplified "regularized variational multiscale model" and an "enhanced field model", Physics of Fluids, 19, 055 110, 2007.

Kinzel, M., Mulligan, Q., and Dabiri, J. O.: Energy exchange in an array of vertical-axis wind turbines, Journal of Turbulence, 13, N38, doi:10.1080/14685248.2012.712698, http://dx.doi.org/10.1080/14685248.2012.712698, 2012.

Koumoutsakos, P.: Inviscid axisymmetrization of an elliptical vortex, Journal of Computational Physics, 138, 821–857, doi:http://dx.doi.org/10.1006/jcph.1997.5749, 1997.

Koumoutsakos, P.: Multiscale flow simulations using particles, Annual Review of Fluid Mechanics, 37, 457–487, 2005.

Leishman, J. G.: Principles of helicopter aerodynamics, Cambridge University Press, 2nd edn., 2006.

Leweke, T., Le Dizès, S., and Williamson, C. H. K.: Dynamics and Instabilities of Vortex Pairs, Annual Review of Fluid Mechanics, 48, 507–541, doi:10.1146/annurev-fluid-122414-034558, http://dx.doi.org/10.1146/annurev-fluid-122414-034558, 2016.

Litvinov, I., Naumov, I., Okulov, V., and Mikkelsen, R. F.: Comparison of far wakes behind a solid disk and a three-blade rotor, Journal of Flow Visualization and Image Processing, 22, 2015.

Migliore, P. and Wolfe, W.: Some effects of flow curvature on the performance of Darrieus wind turbines, American Institute of Aeronautics and Astronautics, doi:doi:10.2514/6.1979-112, http://dx.doi.org/10.2514/6.1979-112, 1979.

Monaghan, J.: SPH without a Tensile Instability, Journal of Computational Physics, 159, 290–311, 2000.

Monaghan, J. J.: Extrapolating B splines for interpolation;, Journal of Computational Physics, 60, 253–262, http://www.sciencedirect.com/science/article/B6WHY-4DD1WC8-19H/2/5388f2c6dbe3898de31ea0ea7bbb03fa, 1985.

Paquette, J. and Barone, M. F.: Innovative Offshore Vertical-Axis Wind Turbine Rotor Project, in: EWEA 2012, April 16-19, 2012 in Copenhagen, Denmark., EWEA, 2012.

Ploumhans, P. and Winckelmans, G. S.: Vortex Methods for High-Resolution Simulations of Viscous Flow Past Bluff Bodies of General Geometry, Journal of Computational Physics, 165, 354–406, http://www.sciencedirect.com/science/article/B6WHY-45FC88K-3/2/3f55200e6caead3c52ecc8328dfbada8, 2000.

Pope, S. B.: Turbulent flows, IOP Publishing, 2001.

Prandtl, L.: Application of Modern Hydrodynamics to Aerodynamics, Technical Report 116, NACA, 1923.

Scheurich, F.: Modelling the aerodynamics of vertical-axis wind turbines, Ph.D. thesis, University of Glasgow, 2011.

Scheurich, F. and Brown, R. E.: Modelling the aerodynamics of vertical-axis wind turbines in unsteady wind conditions, Wind Energy, 16, 91–107, doi:10.1002/we.532, http://dx.doi.org/10.1002/we.532, 2013.

Scheurich, F., Fletcher, T. M., and Brown, R. E.: The Influence of Blade Curvature and Helical Blade Twist on the Performance of a Vertical-Axis Wind Turbine, in: 48th AIAA Aerospace Sciences Meeting Including the New Horizons Forum and Aerospace Exposition, pp. AIAA 2010–1579, AIAA, 2010.

Sørensen, J. N., Mikkelsen, R. F., Henningson, D. S., Ivanell, S., Sarmast, S., and Andersen, S. J.: Simulation of wind turbine wakes using the actuator line technique, Proceedings of the Royal Society of London. Series A, Mathematical and Physical Sciences, 373, doi:10.1098/rsta.2014.0071, 2015.

Tennekes, H. and Lumley, J. L.: A First Course in Turbulence, MIT Press, https://books.google.be/books?id=h4coCj-lN0cC, 1972.

van Rees, W. M., Leonard, A., Pullin, D. I., and Koumoutsakos, P.: A comparison of vortex and pseudo-spectral methods for the simulation of periodic vortical flows at high Reynolds numbers, Journal of Computational Physics, 230, 2794–2805, 2011.

Williamson, J. H.: Low-storage Runge-Kutta schemes, Journal of Computational Physics, 35, 48–56, http://www.sciencedirect.com/science/article/B6WHY-4DD1NRP-H1/2/a1a09857d87c5a3538d4800fd648be47, 1980.

Winckelmans, G.: Vortex Methods, in: Encyclopedia of Computational Mechanics, edited by Stein, E., De Borst, R., and Hughes, T. J., vol. 3, John Wiley and Sons, 2004.